Enhanced CO$_2$ Emissions Driven by Flooding in a Simulation of Palsa Degradation

Laurent Mélissa[1,6], Baysinger Mackenzie R.[1,6], Schaller Jörg[2], Lück Matthias[2], Hoffmann Mathias[2], Windirsch Torben[1,3,5], Ellerbrock Ruth H.[2], Strauss Jens[1], and Treat Claire C.[1,4]

[1]Alfred Wegener Institute Helmholtz Centre for Polar and Marine Research, Permafrost Research Section, Telegrafenberg, Potsdam, Germany
[2]Leibniz-Center for Agricultural Landscape Research (ZALF), Müncheberg, Germany
[3]Institute of Geosciences, University of Potsdam, Potsdam, Germany
[4]Center for Landscape Research in Sustainable Agricultural Futures, Aarhus University, Denmark
[5]Research Institute for Sustainability Helmholtz Centre Potsdam, Potsdam, Germany
[6]Institute of Geo-ecology, University of Potsdam, Potsdam, Germany

Correspondence: Laurent Mélissa (melissa.laurent@awi.de)

Abstract. Climate change is predicted to put most of the permafrost habitats in the discontinuous zone at risk of disappearing within the next few decades. On a decadal scale, abrupt permafrost thaw may result in larger C losses than gradual permafrost thaw, but drivers of C emissions are poorly understood. To investigate this, we measured C emissions from a palsa under simulated abrupt and gradual thaw scenarios. We continuously measured CO$_2$ and CH$_4$ emissions while deepening the permafrost table under flooded (abrupt) and non-flooded (gradual) conditions. Higher soil-moisture during permafrost thaw is commonly associated with decreasing CO$_2$ and increasing CH$_4$ emissions. Interestingly, our results showed consistent CH$_4$ uptake across all the cores from the palsa and a twofold increase in CO$_2$ emissions under abrupt thaw (flooded conditions). Peat quality analysis (FTIR) showed a higher degradation of C compounds at the permafrost table, likely due to the physical disruption of soil organic matter and the redox changes in the active layer caused by flooding. Averaged CO$_2$ emissions were significantly higher under abrupt thaw (150 mg-CO$_2$ m^{-2} h^{-1}) compared to gradual thaw (70 mg-CO$_2$ m^{-2} h^{-1}), with limited permafrost peat contribution. Conversely, permafrost thaw under gradual thaw contributed to a twofold increase in CO$_2$ emissions (57 to 98 mg-CO$_2$ m^{-3} h^{-1}). Finally, CO$_2$ emissions increased with depth in saturated fens, suggesting that deep-rooted vegetation could be a transport pathway for CO$_2$ outside the growing season. Our findings underline the potential for increased CO$_2$ emissions during the transition to fen conditions under abrupt thaw scenarios and therefore the need for in-situ measurements.

1 Introduction

Peatlands are major terrestrial carbon (C) sinks composed of partially decomposed organic matter (OM). Northern peatlands store approximately 415 ± 150 Pg of C, with 46% (185 Pg C) located in permafrost-affected regions (Hugelius et al., 2020). Decomposition of C is limited due to the frozen and saturated soil conditions that are characteristic of permafrost peatlands. These soil conditions promote C accumulation, while suspending the decomposition of lower layers of OM (Frolking and Roulet, 2007; Sannel and Kuhry, 2009; Turetsky et al., 2000). Permafrost-affected peatlands are particularly vulnerable to shifts in climatic conditions. In the discontinuous permafrost zone, permafrost forms as peat plateaus and palsa - round or elongated permafrost peat mound, maximum height of about 10 m, composed of frozen peat uplifted by ice lenses overlying mineral soil (Seppälä, 1986).

The Arctic is a dynamic and quickly changing biome, with a projected circum-polar temperature increase that is three to four times faster than the global average (Obu et al., 2019; Rantanen et al., 2022; Smith et al., 2022). Climate change in northern Finland is expected to increase precipitation and temperature resulting in a near-complete loss (98.2%) of suitable conditions for palsas by 2080 (Borge et al., 2017; Fewster et al., 2022; Könönen et al., 2022). The loss of palsas will ~~considerably change the vegetation~~ switch vegetation to deep-rooted plants such as sedges, change hydrology by increasing soil moisture (Hugelius et al., 2020; Malhotra and Roulet, 2015). Those changes modify C cycle dynamics, ~~hydrology and C cycle ,~~ altering the C storage capacity of the ecosystem across the discontinuous permafrost zone (Hugelius et al., 2020; Kurylyk et al., 2016; Olefeldt et al., 2021).

During thaw processes, previously frozen soil rejoins the surrounding wetland. This newly thawed material becomes a deeper active layer and generally allows OM to be more readily accessible to microbial organisms (Schuur et al., 2008; Turetsky et al., 2002). This disturbance is known to result in increased mineralization of C as greenhouse gasses, such as carbon dioxide (CO_2) and methane (CH_4) (Kirkwood et al., 2021; Treat et al., 2014; Turetsky et al., 2002). Since it is usually almost entirely OM, C loss in permafrost peatland soils is also strongly affected by the degree of decomposition of the peat and the peat (Jones et al., 2017; Treat et al., 2014), making potential C loss estimates more complex.

The vertical dynamics of C decomposition in permafrost peatlands are especially not yet well understood. Earlier studies found net C accumulation following thaw in newly accumulated surface peat (Camill, 1999; Turetsky et al., 2007). However, more recent projections suggest that permafrost thaw could result in up to 30% soil C loss from the deeper, pre-thaw soil C stock (Hugelius et al., 2020; Jones et al., 2017). This would result in a net C loss for decades to centuries (Hugelius et al., 2020; Jones et al., 2017) or a balanced C system where increased productivity offsets decomposition (Heffernan et al., 2020). Incubation experiments simulated permafrost thaw to assess vertical ~~C~~ OM decomposition over the thaw transect by measuring ~~C~~ gas (CO_2 and CH_4) production at specific depths ~~(?Hodgkins et al., 2014; Kirkwood et al., 2019; Treat et al., 2014, 2015)~~ (Baysinger et al., 2025; Hodgkins et al., 2014; Kirkwood et al., 2019; Treat et al., 2014, 2015). They measured higher CO_2 production from the surface active layer than from the permafrost. Incubation studies generally agree that there is an increase in CO_2 production along the thaw stages ~~(?Hodgkins et al., 2014; Kirkwood et al., 2019; Treat et al., 2014, 2015)~~ (Baysinger et al., 2025; Hod . Additionally, permafrost layers contributed up to 40% of the total CO_2 production (including the active layer), even under

anaerobic conditions. Field measurements, in contrast, indicate permafrost C contribution under dry conditions only, with most C contributions coming from the decomposition of modern C (Estop-Aragonés et al., 2018a; Cooper et al., 2017). In addition, via new peat accumulation vegetation and water-logged soils in thermokarst fens offset C emissions from collapsing palsas, resulting in a C sink, contrasting with findings from more recent projections (Hugelius et al., 2020; Jones et al., 2017). Still,

55 despite new peat accumulation, projections of peat C loss with warming and permafrost thaw range from 3.0 kg C m^{-2} to 36 kg C m^{-2} (Hugelius et al., 2020; Jones et al., 2017; Treat et al., 2021).

The discrepancies between laboratory incubations, on-site field measurements, and model projections highlight potential methodological limitations, particularly the need to study the whole peat profile. Indeed, incubations isolate layers of soil, often homogenizing them and thereby disturbing the soil matrix (Treat et al., 2015), which does not allow for accurate C emis-

60 sion quantification. While field conditions preserve the soil structure, simulating permafrost thaw under controlled conditions is nearly impossible. Field-based chronosequences of permafrost thaw can show the different thaw stages in permafrost peatlands that usually happen over several decades or centuries. However, chronosequence approach makes it difficult to study the transitions between thaw stages and to isolate specific processes. Mesocosm incubations combine controlled conditions with in-situ soil structure and could offer more realistic C loss estimates (Voigt et al., 2019). To our knowledge, only one recent

65 study has simulated thaw in permafrost peatlands with mesocosm incubations. While the authors focused on vegetation and soil moisture, it emphasizes the need to better understand the links between C cycling and hydrology in permafrost peatlands (Voigt et al., 2019).

Thaw can proceed gradually over decades or abruptly within days to years, with the latter often forming thermokarst ponds at collapsing palsa edges (Quinton and Baltzer, 2013; Jorgenson et al., 2006; Borge et al., 2017). Abrupt thaw has recently been

70 more precisely defined as occurring within 30 years in ice-rich soils (>20%) and/or when causing major ecological or state shifts such as wildfire or streamflow changes (Webb et al., 2025). This definition incorporates not only a temporal criterion but also environmental and soil factors such as hydrology and rapid soil moisture increase. With this updated definition, abrupt thaw appears to be the dominant form of permafrost degradation in palsas. In palsa mires, permafrost degradation leads to ground subsidence and hydrological changes, driving the transition from elevated palsas to wetter peatland ecosystems such as bogs and

75 fens (Hugelius et al., 2020). ~~Thaw can proceed gradually over decades or abruptly within days to years, with the latter often forming thermokarst ponds at collapsing palsa edges (Quinton and Baltzer, 2013; Jorgenson et al., 2006; Borge et al., 2017).~~ Additionally, studies from Fennoscandia estimated palsa degradation rates between -1.0 % yr^{-1} and -1.3 % yr^{-1} over the period of 1950/60-2010/2014 (Borge et al., 2017; Leppiniemi et al., 2025; Olvmo et al., 2020) with palsa losses reaching up to 80 % between 2007 and 2021 in specific areas such as Finnish Lapland. Permafrost degradation was primarily attributed to

80 palsa collapse rather than active layer deepening (Verdonen et al., 2023).

Although abrupt thaw affects a smaller area, it may contribute to permafrost C release- up to 40%— yet is underrepresented in Earth System Models, particularly regarding associated hydrological changes (Turetsky et al., 2020; Rodenhizer et al., 2023b). Most studies on abrupt vs. gradual thaw have focused on steady-state outcomes—dried peatlands or stabilized thermokarst features—measuring C release under either aerobic (gradual) or anaerobic (abrupt) conditions, with the latter

85 typically showing lower CO_2 emissions (?Harris et al., 2023; Hodgkins et al., 2014; Kirkwood et al., 2021; Jones et al., 2017)

(Baysinger et al., 2025; Harris et al., 2023; Hodgkins et al., 2014; Kirkwood et al., 2021; Jones et al., 2017). As a result, microbial, physical, and redox processes during the transitional thaw stage remain poorly understood. In transitional stages, soils are newly flooded yet not fully anoxic and this may also increase in-situ CO_2 emissions, as it has been measured in thermokarst (Kuhn et al., 2018; Matveev et al., 2016; McGuire et al., 2009; Rodenhizer et al., 2023b). During thaw transitions, interactions between collapsing palsas and adjacent fens create distinct redox conditions in thermokarst ponds, making the OM more available for microbial degradation (Patzner et al., 2020). Thermokarst ponds also support diverse microbial communities, favoring C mineralization (Crevecoeur et al., 2015; Leroy et al., 2025; Peura et al., 2020). In addition, flooding can enhance the vertical and lateral transport of labile carbon, temporarily increasing CO_2 emissions (Van Gestel et al., 1993; Kim et al., 2010). Most of these microbial, physical, and redox processes have been observed primarily under in-situ conditions, making it difficult to isolate specific drivers.

To understand how hydrological changes during abrupt and gradual permafrost thaw influence C emissions in palsa degradation, we incubated meter-long peat cores (mesocosms) from a Finnish palsa mire. Mesocosm incubations preserve in-situ soil horizon structure while maintaining a high-level of control over environmental conditions. With this setup, we simulated abrupt and gradual permafrost thaw under different hydrological conditions using thermokarst pond water to assess microbial and redox influences on C release. We continuously monitored CO_2 and CH_4 emissions and measured peat decomposition using Fourier Transform Infrared (FTIR) spectroscopy. ~~We also~~ In addition, we incubated mesocosms from a post-thaw fen to assess the long-term vs. short-term thaw effects on C releases.

Based on this design, we hypothesized that (H1) flooding with abrupt thaw alters vertical C dynamics by physically disturbing the soil matrix and changing the redox properties of the soil to anaerobic conditions. Anaerobic conditions under the abrupt thaw simulations result to lower CO_2 emissions compared to gradual thaw. (H2) The addition of thermokarst pond water during the thaw simulation enhances C emissions through increase microbial activity due to microbial colonization from the thermokarst pond water. (H3) Long-term thaw in the fen results in higher C emissions than in the palsa because of fresh organic matter input, permafrost-free conditions for several decades and therefore already established microbial communities. The in-situ water logged conditions in the fen site allow for CH_4 emissions during the incubation, while under abrupt thaw simulation, ideal redox conditions are not reached after three-month incubation despite water saturation and therefore no CH_4 emission occurs.

2 Methods

2.1 Study site

We collected cores for the mesocosm incubations from a palsa mire located in a discontinuous permafrost area in the Finnish part of Sápmi in March 2023. The Peera palsa mire (68.8778°N; 21.0792°E) is composed of four palsas (Verdonen et al., 2023), surrounded by fens. The mean annual air temperature measured at the Kilpisjärvi station is -1.7 °C, and the average annual precipitation (rain and snow) is 546 mm (1991–2020, FMI, 2024). In this study, we focused on the southernmost landform (Fig. 1). Over more than 60 years of aerial imagery monitoring, the palsa has lost 77% of its surface area, transitioning into
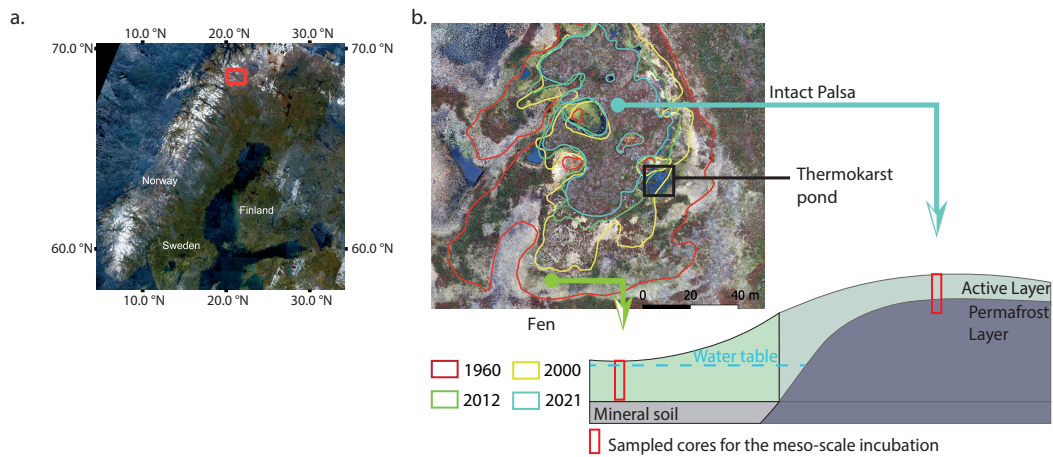
Figure 1. Location of the Peera palsa study site. Aerial image of Finland (Sentinel-2 Mosaics, Copernicus) with the site marked by a red square (a); Aerial view of the palsa (Verdonen et al., 2023) and schematic of the topography and sampling locations for the mesocosm incubation. Lines on the aerial view show the extent of the palsa at different years (b).

thermokarst bog and fen habitats. This transition is associated with a shift in vegetation from shrub-dominated peat to open
120 water, followed by colonization by *Sphagnum* mosses and sedges (Verdonen et al., 2023). Based on the definitions from Peura et al. (2020), the palsa is surrounded by three developing thermokarst ponds and four emerging ponds at its edge. The thermokarst ponds are located at the same elevation as the surrounding fen, which lies approximately two meters lower than the palsa. We measured a peat thickness of 1.7 m and an active layer depth of 60 cm at the top of the Peera palsa dome. The active layer was measured during the first ~~sampling~~ exploratory expedition in October 2022. Since this was at the end of the
125 growing season, we assume this represents the maximum annual active layer depth. The vegetation at the sampling locations on Peera palsa is characterized by shallow-rooted species such as *Betula nana subsp.*, *Empetrum nigrum subsp.*, and *Vaccinium myrtillus*, while the surrounding fen is dominated by deep-rooted vegetation such as *Eriophorum*, *Sphagnum*, and sedges (Fig. S1).

2.2 Sampling of peat mesocosms and water

130 We sampled cores from two thaw stages: the intact palsa and the thermokarst fen (Fig. 1). To minimize soil disturbance, sampling was conducted in winter (March 2023), when frozen conditions help preserve water content and prevent artificial compaction. We collected twelve cores (1 m long, 7.5 cm diameter) from the Peera palsa and three from the fen (Fig. 1). At both sites, we also collected a 'long core' down to mineral soil for sedimentary analysis. Mesocosms from the palsa were drilled using a ~~modified~~ snow, ice, and permafrost (SIPRE) auger (Jon's Machine Shop, Alaska, USA). In the fen, only the top
135 15 cm were frozen, so we used the SIPRE auger for that layer and then drove a metal pipe into the unfrozen soil to complete the core. To preserve soil structure, the pipes were frozen vertically. We wrapped the palsa samples and the frozen top layers from the fen in core foil and stored them in thermoboxes.

We collected 45 L of water from a thermokarst pond adjacent to the palsa (68.8775°N; 21.0798°E), using pre-cleaned 10 L canisters. We drilled through the surface ice with the SIPRE auger before sampling.

140 Samples were stored at -20°C at the Kilpisjärvi Research Station during the expedition. They were later shipped frozen to AWI in Potsdam, Germany, using a refrigerated truck and stored at -20 °C until the start of the experiment.

2.3 Mesocosm set-up

2.3.1 General setup

This study aimed to quantify CO_2 and CH_4 emissions under both abrupt and gradual permafrost thaw simulations, focusing
145 on hydrological changes during abrupt thaw. We used a mesoscale incubation setup to preserve the in-situ soil structures and allow gas diffusivity in the soil column. We incubated meter-long cores (mesocosms) from the two sampled sites, the palsa and the fen, at 10°C under dark conditions for 12 weeks (Fig. 2). We sequentially thawed permafrost to simulate palsa degradation and applied the same treatment to the fen cores. For all the mesocosms, CO_2 and CH_4 emissions were continuously measured throughout the incubation duration (2.4). The mesocosms from the palsa were exposed to four different treatments
150 simulating gradual and abrupt thaw (see details below). ~~We compared the C emissions from~~ A core from the fen was included as an end-member representing long-term thawed conditions (60 years). This allowed comparison of CO_2 and CH_4 emissions following short-term simulated permafrost thaw with ~~emissions from a long-term thawed fen by incubating mesocosms from the fen site~~ those from a naturally thawed fen. In the field, the water table at the fen site was at the surface (September 2022). Therefore, to best represent in-situ conditions, we kept the water table of the mesocosms from the fen at the surface by adding
155 water from the thermokarst pond. For all the mesocosms, we removed the vegetation at the surface of the core. We used three replicates for each treatment, for a total of fifteen mesocosms.

2.3.2 Gradual vs. Abrupt thaw treatments

We simulated gradual thaw (control treatment; Fig. 2) by incubating mesocosms from the palsa site under in-situ moisture, which was approximately 60% volumetric water content (Fig. S13). When palsas thaw abruptly, soil typically collapses into
160 thermokarst ponds (Fig. 2). To simulate the sudden increase in soil moisture during abrupt thaw, we flooded the mesocosms until the water table reached the surface (0 cm). We chose to flood the mesocosm with a similar water table as the one measured at the fen site to be able to compare emissions from both sites. For both thaw simulations (gradual and abrupt thaw) mesocosms were thawed at the same speed and only the water content was modified. The mesocosms were subjected to three treatments to test the influence of water chemistry and microbes: autoclaved tap water (TW), non-filtered (NF) thermokarst pond water, and
165 filtered (F) thermokarst pond water. The NF treatment exposed the mesocosms to both the microbial and chemical properties of the thermokarst pond water. The F treatment, in which microbes were removed by filtration (SI) from the thermokarst pond water, isolated the chemical properties of the thermokarst pond water. To isolate the effect of flooding on C emissions, we flooded another set of mesocosms with the TW treatment.

2.3.3 Water addition

For all mesocosms under flooded conditions (TW, NF, F, and the fen), we flooded the mesocosms from the side at four different depths (Fig. S5). We added water from the side to avoid preferential vertical pathways. We used Bev-A-Line tubes (Saint-Gobain 06490-12) equipped with three-way valves (Masterflex®-Fitting, MFLX30600-25). ~~Water was added after each thaw stage~~We thawed the samples overnight, and added water the day after. After each thaw stages, we applied the same procedure. Additionally, we ensured the water table remained at the surface by bi-weekly checks and adjusted the level as needed (Fig. S6).

2.3.4 Sequential thawing

All cores were thawed in three steps to assess the contribution of C emissions from the active layer (60 cm thick), which thaws during the growing season, and the permafrost layers. To isolate the effects of hydrological changes between gradual and abrupt thaw, all cores underwent the same permafrost thawing process. The sequential thaw was implemented by exposing the top 60 cm to 10°C for four weeks, ensuring complete thaw of the active layer. The first thaw stage corresponded to the maximal annual active layer depth measured in October 2022, and the incubation temperature (10°C) corresponded to the mean growing season soil temperature. To thaw the permafrost, we deepened the active layer by 20 cm every four weeks (Table S2). The duration of each sequential thaw was determined based on the time need for CO_2 fluxes to stabilize during the first thaw thaw step. For consistency, we applied the same thaw duration for each thaw step. However, we acknowledge that the duration for CO_2 fluxes to stabilize following thaw might have differed for each sequential thaw. The frozen part of the core was kept at -5°C. Due to setup limitations, we also applied the sequential thawing to the mesocosms from the fen, although this did not fully represent field conditions. Quality control of conditions was performed by continuously monitoring the temperature inside the incubator and the soil for one replicate per treatment. The temperature was recorded at five depths (0–20–40–60–80 cm) every half hour using temperature sensors (Hobo U12-008 data logger, Fig. S7).

The details regarding the mesocosms, water preparation and addition, and incubation system can be found in the Supplementary Information (Fig. S3 and Fig. S4).

2.4 CH_4 and CO_2 fluxes

2.4.1 Flow-through steady-state system

We used a flow-through steady-state system to measure the concentrations of CH_4 and CO_2 in the mesocosm headspace. As a reference for flux calculations (Eq. 1), an additional empty incubation vial was included and flushed with ambient air. Each channel was connected to a Picarro G2508 gas analyzer (PICARRO, INC., Santa Clara, USA) and measurements were taken over an eight-minute period. When a mesocosm was being measured, a subsampler redirected air from its headspace to the gas analyzer for concentration analysis. The measured GHG concentrations represent the increased GHG levels in the mesocosm
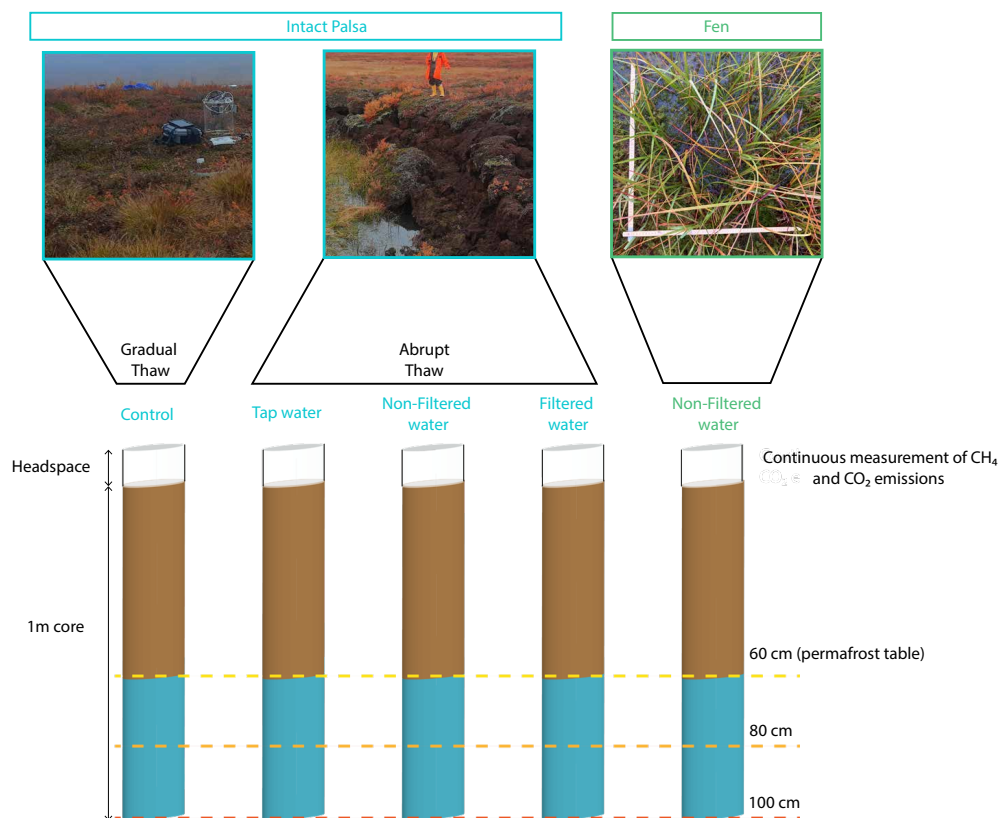
Figure 2. Schematic of the mesocosm setup used for the mesocosm incubation of the samples from Peera, Lapland. The brown part of the cores was directly thawed at the beginning of the incubation, while the blue part was sequentially thawed. For the intact palsa, the blue part corresponds to the permafrost layer. The dashed lines indicate the three thaw stages during the incubation period.

headspace, which reflect both the equilibrium of GHGs emitted from the mesocosm and the replacement of headspace air. At the end of each measurement cycle, the system switched to the next mesocosm, including the reference channel. When not being measured, the mesocosms' headspaces were continuously flushed with a stable flow of ambient air (flow rate = 16 mL.min^{-1}). To prevent desiccation of the mesocosms, the inflow air was saturated with water (Fig. S4).

2.4.2 Quality Control prior to Flux calculations

During incubation, we measured CO_2 fluxes above the gas analyzer's detection limit (5,000 ppm). Fluxes above this threshold saturated the C sensors, rendering the system unable to measure CH_4 emissions. We manually filtered out time windows for each channel where flux anomalies were detected (Supplementary Info, Fig. S5, Table S1). Overall, 11.7% of the data were filtered (Table S1, Fig S18 and S19).

2.4.3 Flux calculations

Data were processed prior to flux calculations. We excluded the first five minutes of each measurement to ensure that we were capturing emissions from the mesocosms, rather than carryover air from the system. C fluxes were calculated as the difference between the C emissions from the mesocosm headspace (outlet) and the reference channel (inlet) over time. The concentrations were converted using the Ideal Gas Law and then multiplied by the flow rate to obtain the fluxes (Mastepanov and Christensen, 2009).

$$F = \frac{\Delta C f p M}{S R T} \tag{1}$$

Where F the flux (mg m^{-2} h^{-1}), ΔC is the difference gas concentration between the measured mesocosm and the reference channel in ppm, f the flow rate (m^3 h^{-1}), p the pressure (Pa), M the molar mass (in mol g^{-1}), S the base area of the mesocosm (in m^{-2}), R the ideal gas constant (m^3 Pa Pa K^{-1} mol^{-1}) and T the incubation temperature (K). We adapted the script from Hoffmann et al. (2017) to calculate the C fluxes.

2.4.4 Quality control post-flux calculation

We identified outliers by applying a rolling Interquartile Range (IQR) with a sliding step of one day. Outlier measurements resulting from laboratory manipulation or technical issues were excluded. After data cleanup, we quantified fluxes below the instrument's detection limit by calculating the Minimum Detectable Flux (MDF) (Nickerson, 2016). The final dataset is available in Laurent et al. (2025a).

2.5 Soil analyses

2.5.1 Sedimentary and pore water analysis

We characterized the sedimentary and geochemical composition (including TOC, TN, conductivity, pH, DOC and water content) of the intact palsa and fen sites using long cores. We thawed the samples at room temperature and extracted the pore water using a rhizon soil moisture sampler (Rhizon MOM 0.6 μm, Rhizosphere Research Product – Meijboom and van Noordwijk, 1991) for two days. We separated the water collected into two 50 mL bottles, one for pH and Electrical Conductivity and the second one for Dissolved Organic C (DOC). EC and pH measurements were conducted by a conductivity pocket meter with a reference temperature of 25 °C (Cond 340i, WTW, Germany) and a potentiometer (Multilab 540, WTW, 125 Germany). The water for DOC was acidified with 30 percent HCl and was analyzed by catalytic combustion at 630 °C (TOC-VCPH,Shimadzu, Japan).

We measured Total Organic Carbon (TOC), Total Carbon (TC), and Total Nitrogen (TN) before and after incubation at five different depths along the core (0 cm, 25 cm, 50 cm, 75 cm, and 100 cm). We used an elemental combustion analyzer (Elementar soliTOC cube) to measure TOC and TC, and a nitrogen analyzer (Elementar rapidMAX N, Germany) to measure TN. We analyzed each subsample in duplicate to ensure precision and used standards and blanks to maintain reliable and accu-

rate analytical measurements. The final dataset reporting the geosedimentology of the samples can be found in Laurent et al. (2025b).

2.5.2 Water content

We measured the initial gravimetric soil water content using the samples collected for sedimentary analysis. We first weighed the samples while they were still frozen, then weighed them again after freeze-drying. We calculated gravimetric soil water content as the mass of water lost divided by the mass of the dried soil.

2.5.3 Fourier Transform Infra Red analysis

We analyzed the same samples as for TOC and TN analyses for FTIR spectroscopy in the KBr technique (Heller et al., 2015; Ellerbrock et al., 2024). The samples were measured at the Leibniz-Zentrum für Agrarlandschaftsforschung, Müncheberg (Germany). We used the average of 16 scans to obtain the spectra (Ellerbrock et al., 2024). Each sample was corrected against ambient air (Haberhauer and Gerzabek, 1999). The baseline corrected spectra (Ellerbrock et al., 1999) were interpreted as described in Ellerbrock and Gerke (2013).

To characterize the peat decomposition, the interpretation of the FTIR spectra focused on absorption bands that reflect the amount of aliphatic (CH) and carboxylic (C=O) groups within the peat samples. The CH band (2900-2700 cm^{-1}) is characteristic of the OM aliphatic backbone (Ellerbrock and Gerke, 2013). While the C=O band (1710-1640 cm^{-1}) reflects the presence of oxidized (carboxyl) groups. A higher intensity in the C=O band signifies increased OM decomposition. CH bands are usually superimposed as a shoulder of the broad OH band which spans 3750-2700 cm^{-1}. The absorption intensities of the CH bands were quantified as the vertical distance from a local baseline (Capriel et al., 1995), which was defined between tangential points on the OH-band (near the wave numbers 3020 and 2800 cm^{-1} (red arrows within the enclosure in Fig. S11; Ellerbrock et al. (2009)). Similarly, the C=O band intensities (black arrows in Fig. S11) were measured as the height from the total baseline to the maxima within wave number ranges 1780–1710 cm^{-1} and 1680–1580 cm^{-1} (Ellerbrock and Kaiser, 2005).

The ratios of specific bands provide insights into OM characteristics. The ratio of C=O to polysaccharide (COC) (C=O/COC ratio) indicates the potential cation sorption capacity (Ellerbrock and Gerke, 2021), while the ratio of CH to COC (CH/COC ratio) reflects the balance between non-oxidized OM and litter OM, serving as a proxy for potential hydrophobicity. To evaluate the decomposition stage of the peat samples caused by incubation process we adopted here a procedure described by Hodgkins et al. (2014) by relating the CH/COC and C=O/COC ratios of the original peat samples with those of the incubated samples (Eq. 2, Eq. 3). One replicate among the three was used for the post-FTIR analysis. The replicate with temperature sensors could not be used due to potential contamination because of the sensors. The third one was kept intact as a backup.

$$\text{DI}_{CH} = \frac{\text{CH/COC}_{\text{after incubation}}}{\text{CH/COC}_{\text{before incubation}}} \tag{2}$$

$$\text{DI}_{C=O} = \frac{\text{C=O/COC}_{\text{after incubation}}}{\text{C=O/COC}_{\text{before incubation}}} \tag{3}$$

With DI_{CH} representing the decomposition indices (DIs) based on changes in the aliphatic backbones, and $\text{DI}_{C=O}$ assessing changes in the carboxylic group content. An index >1 means an increase of the decomposition during the incubation.

2.5.4 ~~Pore water analysis~~

~~For the samples sampled prior to incubation, we additionally measured pH, Electrical Conductivity (EC) and DOC. We thawed the samples at room temperature and extracted the water with rhizons for two days. We separated the water collected into two 50 mL bottles, one for pH and Electrical Conductivity and the second one for DOC. EC and pH measurements were conducted by a conductivity pocket meter with a reference temperature of 25 °C (Cond 340i, WTW, Germany) and a potentiometer (Multilab 540, WTW, 125 Germany). The water for DOC was acidified with 30 percent HCl and was analyzed by catalytic combustion at 630 °C (TOC-VCPH,Shimadzu, Japan)."The final dataset reporting the geosedimentology of the samples can be found in Laurent et al. (2025b).~~

2.6 Data processing and statistical methods

We characterized the thawing response by determining shifts in the emissions over time. To do so, we applied a changing-point-based method coupled to a sliding mean (Rodionov, 2004). When a potential shift is detected, a Student's t-test is run to validate whether the anomaly is statically different from the mean value. We tested the method for several cut-off lengths to cover short-term and long-term regimes. In the end we chose a cut-off length of 5 days. We ran the Rodionov test with the rshift package (Room et al., 2020).

We tested the differences among treatments and thaw stages for the averaged fluxes with a one-way ANOVA coupled to a TukeyHSD test. We also grouped the treatments between flooded and dry conditions and tested for significance. Before performing statistical test, we tested the data for independency, normality and homogeneity of variance. Finally, to ensure that filtering did not affect the statistics, we performed a Kruskal-Wallis test followed by pairwise comparisons using Dunn's test on both the non-filtered (before quality control) and filtered (after quality control) datasets. Because extreme values can strongly influence mean-based comparisons, we employed robust, median-based statistical methods that are less sensitive to outliers to compare the two datasets (Table S4).

We used R ~~(R Core Team, 2024)~~ (R Core Team, 2024) for all the computations.

3 Results

3.1 Soil and Pore Water Characteristics

pH values in the active layer ranged from 3.4 to 3.6. The pH in the permafrost layer was less acidic, with values between 4.2 (~~deepest value~~depth 100 cm) and 4.9 (permafrost table). EC was three times higher in the active layer than in the permafrost layer. As with pH and EC, the DOC concentration increased in the permafrost layer (ranging from 120 to 165 mg·L^{-1} in the active layer and from 402 to 480 mg·L^{-1} in the permafrost layer) (Fig. 3). The pH and EC in the fen core were homogeneous along the soil profile, with pH values similar to those in the permafrost layer and EC values of the same order of magnitude as those in the active layer. Unlike in the palsa, DOC concentration in the fen decreased with depth (Fig. 3). TOC and C:N ratios did not differ between the two sites. TOC values ranged from 41% to 52%, with the lowest values (41%) measured at the permafrost table. The C:N ratios remained consistent along the soil profile (between 30 and 40), with a decrease at the permafrost table and at a depth of 70 cm (16) (Fig. 3).

Overall, we observed a difference between the active and permafrost layers in the soil pore water, while the sediment parameters remained stable along the soil profile. The soil parameters in the fen were mostly stable with depth. Finally, the difference between the palsa and the fen was mainly evident in the composition of the soil pore water.
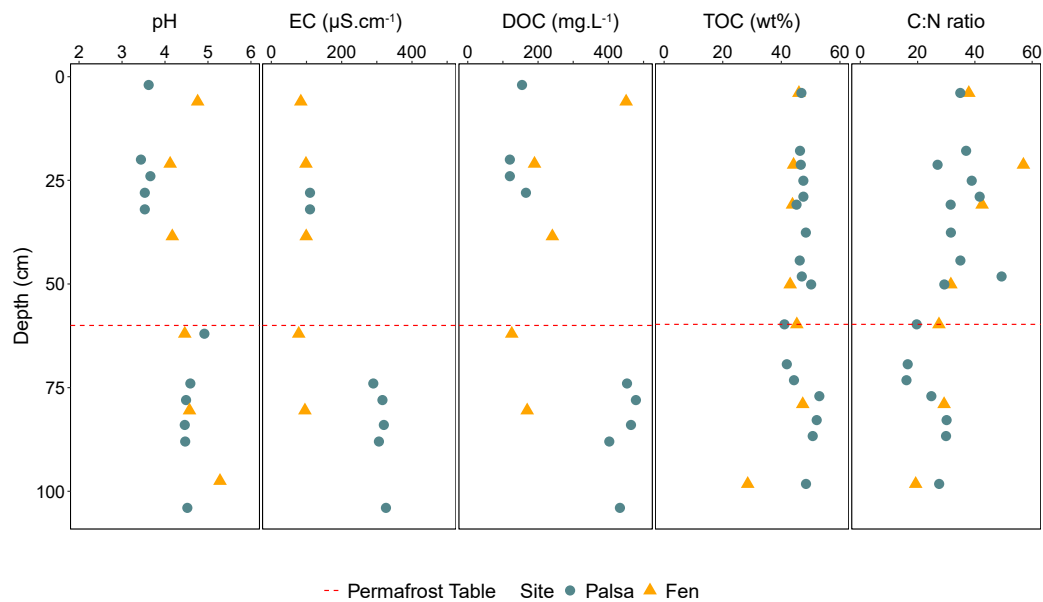
Figure 3. Sediment and soil pore water parameters within the first meter of the palsa and fen prior to incubation. Green circles indicate values measured from the palsa, while yellow triangles represent values from the fen. The red dashed line marks the position of the permafrost table in the palsa.

3.2 FTIR - Organic matter quality and decomposition

The FTIR spectra of the palsa samples collected at 0–2 cm and 18–22 cm depth showed band intensities 15% (0–2 cm) to 30% (18–22 cm) higher for the CH and C=O bands (Fig. 4a – 0 and 20 cm), compared to the fen samples. At 60 cm depth (the permafrost table), the opposite trend was observed (Fig. 4a – 60). No differences were observed in the FTIR spectra of palsa and fen samples collected at 100 cm (Fig. S12). After incubation, the strongest decomposition of OM was observed in samples from the permafrost table (60 cm), with a DI of 1.8 (Fig. 4b). This was also supported by an increase in the band intensities of CH and C=O groups post-incubation (Fig. 4b). The DI ratios in the flooded (abrupt thaw simulation) cores were approximately 1.7 times higher than those in the Control (Fig. 4b; Fig. S12). Little changes were observed in other layers. In the fen cores, the most significant increase in band intensity post-incubation was detected in the bottom layer (100 cm), which also had the highest DI value of 1.9. Above this depth (0–80 cm), little to no change was observed during incubation.

Under in-situ conditions (i.e., prior to incubation), we measured a higher degree of OM decomposition in the active layer of the palsa compared to the fen. After incubation, the depth of greatest OM decomposition varied by site: in the palsa, the permafrost table experienced the highest decomposition, whereas in the fen, most changes in CH and C=O bands occurred in the bottom layer.

3.3 CO$_2$ emission dynamics

3.3.1 Transient palsa thaw vs. stabilized thaw fen incubated under in-situ conditions

During the incubation period, CO$_2$ emissions in the fen mesocosms were consistently three to four times higher than in the Control (Fig. 5, Table 1). The Control reached its highest emissions (233 mg-CO$_2 \cdot$m$^{-2} \cdot$h^{-1}) at the end of the incubation (86 days), whereas the fen attained its maximum (587 mg-CO$_2 \cdot$m$^{-2} \cdot$h^{-1}) after 37 days (Fig. 5).

We observed a CO$_2$ burst from the fen mesocosms during the first seven days, followed by a continuous decrease (Fig. 5, Fig. S14). For the second and third thawing events, a transition period—defined as the period following a thaw event when C emissions decrease or increase before stabilizing—lasted three and two days, respectively. This was marked by a 66% decrease in CO$_2$ emission rates. Following these periods, CO$_2$ emissions increased again and reached a new steady state (Fig. 5). In contrast, in the Control, deepening of the active layer triggered a four-day CO$_2$ burst during the second thaw event (120 mg-CO$_2 \cdot$m$^{-2} \cdot$h^{-1}). Thereafter, emissions returned to a stable rate (15 mg-CO$_2 \cdot$m$^{-2} \cdot$h^{-1}). The transient period during the third thaw event was similar to the fen cores (two days); however, unlike the second thaw event, CO$_2$ emissions increased continuously after the transient period, rising from 51 to 233 mg-CO$_2 \cdot$m$^{-2} \cdot$h^{-1}.

The average CO$_2$ emissions from the Control showed no significant differences between thaw stages (TukeyHSD; p-value > 0.05). However, the last event exhibited a threefold increase in CO$_2$ emissions compared to the second (0–80), due to deepening of the permafrost table (Table 1). When comparing the normalized volume of thawed soil, CO$_2$ emissions were of the same order of magnitude for the first and last thaw stages (0–60: 94.3 ± 26.3 mg-CO$_2 \cdot$m$^{-3} \cdot$h^{-1}; 0–100: 98.3 ± 3.6 mg-CO$_2 \cdot$m$^{-3} \cdot$h^{-1}; Table 2). For the fen, we measured a continuous 85% increase in average CO$_2$ emissions with thaw stage (Table 1) and stable CO$_2$ emissions per volume of thawed soil (Table 2)
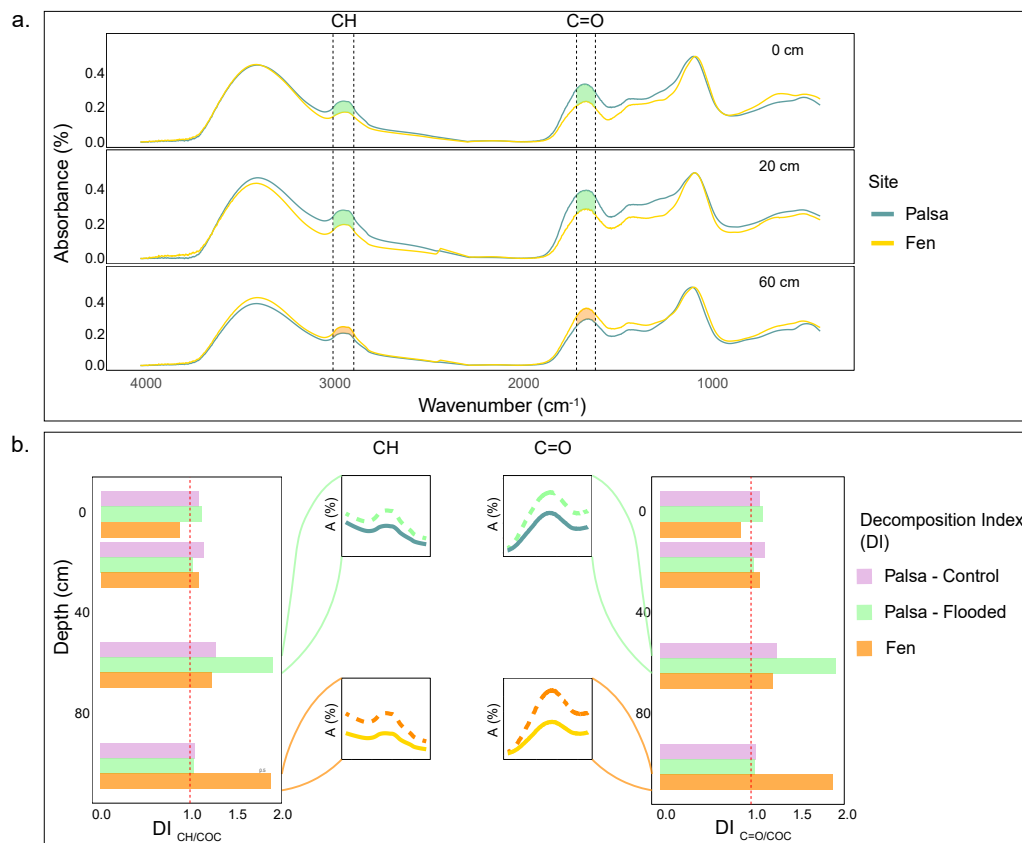
Figure 4. Peat quality along the the soil profile of the palsa and the fen. FTIR spectra of peat samples collected at the palsa and fen sites from 0 to 2 cm (top), 18 to 22 cm (center), and 58 to 62 cm (bottom) (a.); Decomposition Index (DI) of CH/COC (left) and the C=O/COC ratios (right) during incubation were calculated from FTIR data for palsa and fen samples, both before and after incubation (Hodgkins et al., 2014). The zoomed-in spectral sections highlight differences in band intensity before (solid line) and after (dashed line) incubation, focusing on the depth with the greatest increase in degradation (b).

Overall, in mesocosms incubated under in-situ conditions, we observed two distinct behaviors based on site. CO_2 emissions from the Control were significantly lower than those from the fen (TukeyHSD; p-value = 0.0004; Table 1). Finally, we measured a stronger response to thaw deepening in the fen compared to the Control.

3.3.2 Palsa degradation under different hydrological conditions

For the three thaw stage periods, we did not observe significant differences in average CO_2 emissions between the water treatments (TukeyHSD; p-value > 0.05; Table 1, Fig. 6). However, we did observe significant differences when we grouped all the water treatments together, compared to the Control (TukeyHSD; p-value = 0.005; Table 1, Fig. 6). Throughout the incubation, the mesocosms under flooded conditions had emissions two to three times higher than those under control conditions, except
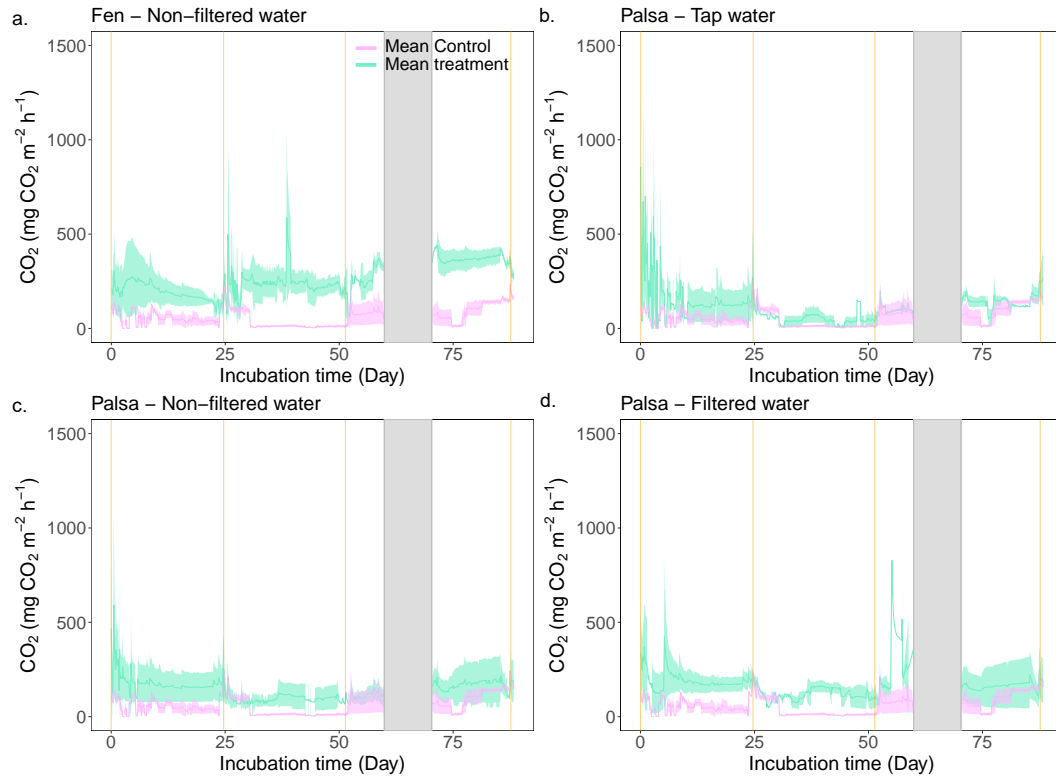
Figure 5. Continuous CO_2 emissions throughout the incubation period. The green line is the average CO_2 emission from the three replicates for the labeled treatment. The purple line depicts the average CO_2 emissions from the Control treatment and is used as a baseline. Finally, the vertical orange lines indicate the thaw stage times and the shaded grey area corresponds to a system failure.

for the Tap water during the second thaw stage (0–80). Emission rates ranged between 120 ± 20.8 mg-$CO_2 \cdot m^{-2} \cdot h^{-1}$ (Filtered - 0–80) and 191.7 ± 57 mg-$CO_2 \cdot m^{-2} \cdot h^{-1}$ (Filtered - 0–60) (Fig. 6, Table 1).

After thawing the active layer, the palsa mesocosms simulating the abrupt thaw (under flooded conditions: Tap water, Non-filtered, Filtered Water) experienced a burst of CO_2 emissions (> 300 mg-$CO_2 \cdot m^{-2} \cdot h^{-1}$ for all three treatments) during the

355   first two to three days (Fig. 5, SI). Afterward, the mesocosms reached stable emissions, ranging from 120 mg-$CO_2 \cdot m^{-2} \cdot h^{-1}$ (Tap water) to 160 mg-$CO_2 \cdot m^{-2} \cdot h^{-1}$ (Filtered water). These emission rates were within the range of CO_2 emissions observed in fen cores during the initial thawing period (Table 1, Fig. 6).

Thawing the permafrost did not result in increased CO_2 emissions for any of the cores under flooded conditions (Table 1, Fig. 6). When normalized by the volume of thawed soil, we measured significantly higher CO_2 emissions during the first thaw stage

360   (0–60) under the abrupt thaw simulation (TukeyHSD; p-value = 0.02; Table 2). For individual water treatments, the highest CO_2 emissions were mainly observed during the first thawing step (0–60 cm), with maximum values for Tap water: 855 mg-$CO_2 \cdot m^{-2} \cdot h^{-1}$ (1-day); Non-filtered: 591 mg-$CO_2 \cdot m^{-2} \cdot h^{-1}$ (1-day); Filtered: 828 mg-$CO_2 \cdot m^{-2} \cdot h^{-1}$ (54-day). In contrast, the distribution of CO_2 emissions for the Control showed higher rates when the entire soil column was thawed (Table 1, Fig.

6). Interestingly, we measured the minimum average CO_2 emissions during the second thawing event (0–80 cm) for all the
365 Palsa cores (Control and Flooded; Table 1).

Similar to the fen, we observed a 60 to 80% decrease in CO_2 emissions following the second thaw stage (0–80) for all
mesocosms under flooded conditions. Two to three days later, CO_2 emissions increased again and eventually reached a new
equilibrium (Fig. 5).

In summary, the flooded palsa cores exhibited CO_2 emissions that were twice as high as the Control cores. However, we did
370 not detect an effect of the different water treatments on the CO_2 emissions. The mesocosms under flooded conditions were not
affected by thaw deepening, while the Control showed higher CO_2 emissions when the entire column was thawed.

Table 1. Average CO_2 and CH_4 emissions for each treatment and site over individual thaw stage. Averages not sharing any letters are significantly different by the Tukey-test at the 5% level of significance.

Site	Treatment	Average CO_2 emissions (n=3) ($mg\text{-}CO_2 \cdot m^{-2} \cdot h^{-1}$)			Average CH_4 emissions (n=3) ($\mu g\text{-}CH_4 \cdot m^{-2} \cdot h^{-1}$)		
		Thaw Stage (cm)					
		0-60	**0-80**	**0-100**	**0-60**	**0-80**	**0-100**
Palsa	Control	56.6 ± 15.8^a	32.8 ± 0.8^a	98.3 ± 3.6^{ab}	-10.8 ± 4.2	-3.2 ± 0.6	-15.5 ± 2.3
	Tap Water	155.8 ± 96.6^{ab}	52.9 ± 17.8^a	144.1 ± 17.9^{ab}	-25.6 ± 26.8	-7.3 ± 7.2	-20.9 ± 6.3
	Non-Filtered Water	178.8 ± 96.1^{ab}	96.1 ± 48.0^{ab}	171.1 ± 90.4^{ab}	-18.1 ± 31.8	-27.9 ± 18.5	-34.6 ± 15.4
	Filtered Water	191.7 ± 57.9^{ab}	120.8 ± 20.8^{ab}	163.5 ± 102.4^{ab}	-33.0 ± 21.4	-31.1 ± 17.1	-25.1 ± 21.2
Fen	Non-Filtered Water	194.8 ± 74.9^{ab}	240.5 ± 50.4^{bc}	368.1 ± 39.6^c	9.7 ± 17.8	-33.5 ± 2.9	-53.9 ± 4.1

Table 2. Average CO_2 and CH_4 emissions for each treatment and site over individual thaw stage normalized by volume of thawed soil. Averages not sharing any letters are significantly different by the Tukey-test at the 5% level of significance.

| Site | Thaw simulation | Average CO_2 emissions (n=3) ($\text{mg-CO}_2 \cdot \text{m}^{-3} \cdot \text{h}^{-1}$) Thaw Stage (cm) | | |
		0-60	0-80	0-100
Palsa	Control	94.3 ± 26.3^{ab}	40.9 ± 0.9^{a}	98.3 ± 3.6^{ab}
	Flooded	292.4 ± 126.2^{d}	112.4 ± 50.8^{ab}	159.6 ± 69.9^{bc}
Fen	None	324.6 ± 124.8^{cd}	300.6 ± 63.0^{cd}	368.1 ± 39.4^{d}
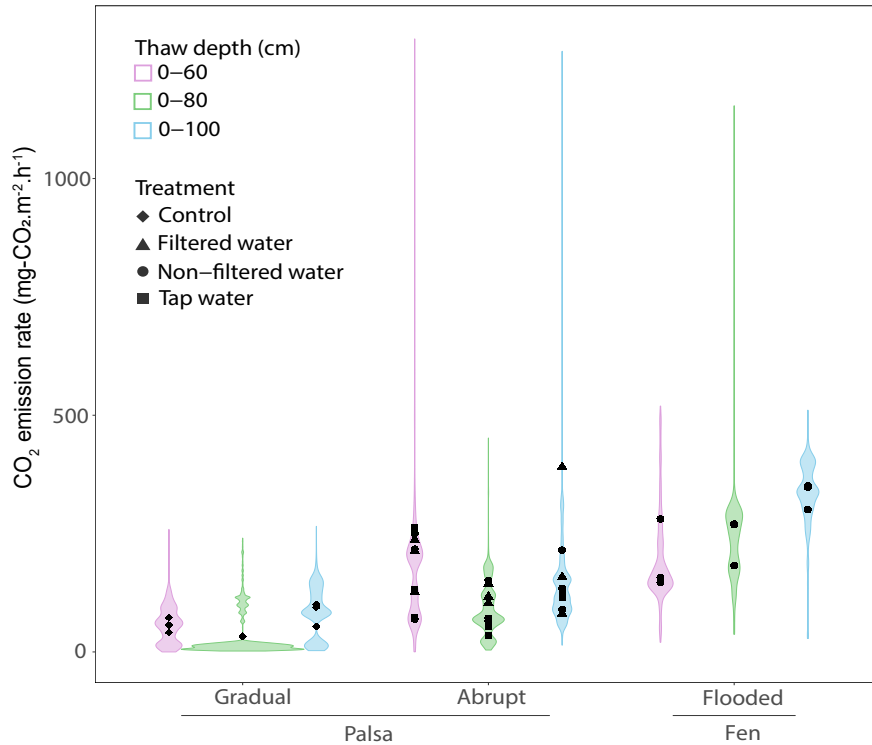
Figure 6. CO_2 emissions rates for each thaw stages under flooded or controlled conditions. The distribution uses the time series data of CO_2 emissions from each thaw stage, under conditions (control vs. flooded) and across sites (palsa vs. fen) to create the violin plots with the points indicating the average CO_2 emissions for each treatment. The colors show the different thaw stage events.

3.4 CH_4 emission dynamics

The palsa mesocosms exhibited a net uptake of CH_4 for all treatments (ranging from -3.2 ± 0.6 to -34.6 ± 15.4; respectively Control-0–80 and Non-Filtered 0–100). Neither the thaw stages nor the treatments had a discernible effect on the CH_4 uptake

375   rates (TukeyHSD, p-value > 0.05; Table 1).

For the fen, we observed a burst of CH_4 emissions during the first week of incubation, followed by emissions close to zero (Fig. S15). This resulted in an average CH_4 emission of 9.7 ± 17.8 $\mu g\text{-}CH_4 \cdot m^{-2} \cdot h^{-1}$ during the first thaw stage (0–60). The second thaw stage (0–80) triggered another burst of CH_4 emissions for three days, while no change in CH_4 emissions was observed after the third stage (Fig. S15). In the fen, the average CH_4 emissions for each thaw stage indicated a continuous increase in

380   CH_4 uptake throughout the incubation period (Table 1, Fig. S15).

4 Discussion

4.1 Environmental conditions driving higher CO_2 emissions in the fen

During the incubation, we measured CO_2 emissions that were three to four times higher in the fen compared to the palsa when the cores were incubated under in-situ moisture conditions (Fig. 5a, Table 1). Our results align with previous incubation studies showing two to four times higher CO_2 production rates from fens than from palsas (?Kirkwood et al., 2021; Kjær et al., 2024) (Baysinger et al., 2025; Kirkwood et al., 2021; Kjær et al., 2024). However, since we removed vegetation from the top layer, the CO_2 emissions we measured were likely higher than under true in-situ conditions, especially for the fens, which typically act as a C sink during the growing season (Holmes et al., 2022; Hugelius et al., 2020). For comparison, Voigt et al. (2017) found that seasonal CO emissions were about three times higher under bare conditions than under vegetated conditions in a warmed treatment. Under control conditions, vegetated sites acted as a CO_2 sink during July and August, while bare sites remained a CO_2 source throughout the snow-free season.

The accumulation and decomposition of peat at the studied sites are shaped by distinct hydrological conditions. The fen site has been permafrost-free for approximately 25 years, in the uppermost 2.5 meters (since 2000), during which the top 23 cm of peat has accumulated (Fig. 1; Reif (2023); Verdonen et al. (2023)). This layer consists of modern C inputs from fresh vegetation. Under water-saturated conditions, decomposition is limited by the lack of terminal electron acceptors (TEAs) (Reddy and DeLaune, 2008), which leads to a higher accumulation of OM (Lee, 1992; Turetsky et al., 2000). In contrast, the active layer of the palsa contained OM deposited over the last 4,600 years and was exposed to decomposition due to dry conditions (Reif, 2023). This prolonged exposure to decomposition in the active layer of the palsa reduced the potential C loss from this site over time (Treat et al., 2021). Our FTIR results indicate that the OM in the active layer of the palsa, prior to incubation, is more decomposed than the OM in the first 60 cm of the fen, reflecting the different hydrological conditions (Fig. 4a) and OM inputs. The dry soil conditions in the palsa led to a shrub-dominated environment with a dried *Sphagnum* layer at the surface. This type of vegetation is typically associated with acidic soils, (pH <4), and our pH results (from 3.4 to 3.6) for the active layer fall into the range of magnitude of palsas (Hodgkins et al., 2014; Kirkwood et al., 2021; Treat et al., 2015). However, *Sphagnum* moss is difficult to decompose because it captures carbohydrates and releases organic acids that inhibit decomposition, which decreases the lability of OM (Mellegård et al., 2009; Zaitseva et al., 2010). The shift from *Sphagnum* to sedge-dominated peat in the fen caused an increase in pH that facilitates OM degradation. Additionally, we measured DOC concentrations that were 2.5 times higher (up to 500 mg.L^{-1}) in the first 20 cm of the fen core (Fig. 3, Fig. S21). DOC from sedge-dominated peat is more labile than DOC from shrub-dominated peat (Chanton et al., 2008). Therefore, we observed a surface layer in the fen with higher and more labile DOC, which could explain the higher CO_2 emissions measured during the incubation.

To summarize, although aerobic conditions facilitate OM decomposition in the palsa, the high degree of peat decomposition combined with low OM inputs has resulted in more recalcitrant OM in the active layer of the palsa (Fig. 4a), potentially limiting further C mineralization (Harris et al., 2023). In contrast, while the fen is O_2-limited, the vegetation, fresh OM input, and adapted microbial communities led to threefold higher CO_2 emissions.

4.2 Increase in CO$_2$ emissions after flooding, simulation of abrupt thaw

In our experimental setting, abrupt thaw simulations resulted in a 55% increase in CO$_2$ emissions under flooded conditions compared to gradual thaw simulations (Control) (Table 1, Fig. 6). These results indicate that the abrupt flooding scenario had a greater impact on CO$_2$ emissions than permafrost thaw alone. This contrasts with previous incubation studies simulating permafrost thaw in palsa, where lower CO$_2$ production was observed under anaerobic conditions ~~(?Treat et al., 2014)~~ (Baysinger et al., 2025; Treat et al., 2014). However, Voigt et al. (2019), in their mesocosm study, did not observe a significant difference in CO$_2$ emissions between flooded and in-situ moisture conditions. Under in-situ moisture conditions, the first 60 cm of the palsa remained aerobic. Therefore, even under flooded conditions, the meso-scale of our experiment delayed the establishment of anaerobic conditions compared to traditional incubations. After a three-month incubation, the flooded palsa mesocosms at 10°C had not reached anaerobic conditions, which also explains the absence of CH$_4$ emissions. ~~Longer mesocosm incubations across different sites are needed to determine how long it takes to fully deplete O$_2$ from the soil column~~Under field conditions, chronosequence studies have shown that CH$_4$ emissions increase during the young and intermediate thaw stages (approximately 10-60 years after thaw), when soils are wetter and vegetation is adapted to these conditions. The lack of anaerobic conditions in our mesocosms likely reflects the short experimental duration compared to natural thaw dynamics (three months vs. several decades). As bogs mature and peat accumulates, the water table lowers, leading to drier conditions and a subsequent decline in CH$_4$ emissions (Johnston et al., 2014; Heffernan et al., 2022, 2024). Additionally, higher CO$_2$ emissions under flooded conditions have also been observed in field studies during the first years after thaw (< 4 years) (Kuhn et al., 2018; Rodenhizer et al., 2023a), supporting the potential for increased CO$_2$ emissions with higher moisture content when O$_2$ remains available.

In their review paper, Kim et al. (2010) compiled studies from various experimental setups and soil types to explain the observed increase in CO$_2$ emissions under flooded conditions. They attributed this increase to higher C lability during flooding events, driven by several mechanisms: (1) changes in soil redox properties (Chen et al., 2020; Patzner et al., 2020), (2) vertical substrate mobilization (Xiang et al., 2008), (3) increased microbial biomass C (Clein and Schimel, 1994; Fierer and Schimel, 2003), and (4) physical disruption, which makes soil OM more accessible (Denef et al., 2001). However, the latter mechanism is likely a minor contributor in peat soils, due to their low mineral content, which limits aggregate formation (Han et al., 2016). The sudden increase in soil moisture with flooding changes the availability of TEAs~~. Palsas, being~~, changing the redox status and reducing the likelihood of CH$_4$ production. Some palsas are iron-rich environments, ~~render iron a crucial TEA (Patzner et al., 2020). Under aerobic conditions, Fe–OM bonds~~ which can help protect OM from decomposition ~~. However, the addition of water can reduce~~ under aerobic conditions but under anaerobic conditions, Fe(III) can be reduced to aqueous Fe(II), thereby making OM more accessible for microbial decomposition (Chen et al., 2020; Patzner et al., 2020). However, other more favorable TEAs such as NO$_3^-$ could be used first to decompose OM and therefore delay the utilization of Fe(III).

Furthermore, flooding stimulates vertical transport within the soil column, mobilizing OM and nutrients from deeper layers to the surface, which can enhance C mineralization (Xiang et al., 2008). In both scenarios, we observed the greatest increase in OM decomposition at the permafrost table (Fig. 4b). However, decomposition was more pronounced under flooding conditions

(DI: 1.9 vs. 1.3 in flooded and control treatments, respectively; Fig. 4b). With enhanced vertical transport, freshly decomposed substrates can be mobilized to upper soil layers (Tfaily et al., 2018).

450 Rewetting soil can also lead to microbial cell lysis, releasing nutrients and increasing microbial biomass (Clein and Schimel, 1994; Fierer and Schimel, 2003; Kim et al., 2012). Most studies reporting CO_2 increases due to cell lysis have observed a short CO_2 pulse lasting up to three days following the rewetting event (Clein and Schimel, 1994; Fierer and Schimel, 2003; Kim et al., 2012). Additionally, because we collected our cores during winter, both the soil and microbial communities were subject to freeze–thaw disruption, which could induce thermal shock and amplify cell lysis. In our study, CO_2 released from

455 microbial biomass could partly explain the pulses observed during the first two to three days of incubation, rather than the overall elevated emissions (Fig. 5). ~~These~~ CO_2 pulses following thaw could also be related to releases of trapped CO_2. Finally, these CO_2 pulses may also be enhanced by physical disturbances due to sequential thawing and, therefore, may not represent natural processes. However, since all the mesocosms were thawed under similar conditions, potential releases of trapped CO_2 or physical disturbances due to setup limitations should be comparable across mesocosms (excluding micro-scale spatial

460 heterogeneity).

The lack of significant differences between water treatments during incubation (Fig. 6, Table 1) is likely due to the overriding effect of water saturation itself, which may have superseded any potential influence of varying water compositions. Additionally, the DOC content of the added water was an order of magnitude lower than that of the palsa and fen soils (9.68; Table S3), thereby reducing the impact of waterborne OM on CO_2 emissions. ~~?~~ Baysinger et al. (2025) reported a 60% decrease in

465 CO_2 production in the permafrost layer under the non-filtered treatment compared to sterile water over a 384-day incubation, likely due to the establishment of anaerobic conditions and the absence of vertical transport. In contrast, our results consistently show approximately twofold higher CO_2 emissions under flooded conditions. We attribute this primarily to vertical substrate mobilization, residual O_2 within the soil column, or redox shifts driven by increased water content, rather than to microbial or chemical inputs from thermokarst pond water. Nonetheless, methodological factors—such as the lateral mode of water addition

470 and data filtering—may have influenced the observed treatment effects.

Finally, we observed CH_4 uptake ranging from 15 to 34.6 μg-CH_4 -m^{-2} -h^{-1} (Table 1, ~~SI~~Fig. S15), even under flooded conditions — consistent with findings by Voigt et al. (2019), who reported uptake ranging from 0.35 to 2.42 mg-CH_4 -m^{-2} -d^{-1}. This observation aligns with results from smaller incubation studies that reported little to no CH_4 production in the active layer ~~(?Kirkwood et al., 2021; Treat et al., 2014)~~(Baysinger et al., 2025; Kirkwood et al., 2021; Treat et al., 2014). We attribute the

475 observed CH_4 uptake to methane oxidation within the soil column, likely facilitated by the presence of residual O_2. Under in situ conditions, the active layer tends to remain dry and oxygenated, which inhibits CH_4 production.

~~This effect was observed throughout the~~ Palsas in Fennoscandia experience degradation rates that vary between -1.0 % yr^{-1} and -1.3 % yr^{-1} over the period of 1950/60-2010/2014 (Borge et al., 2017; Leppiniemi et al., 2025; Olvmo et al., 2020). Palsa collapse has been identified as a major driver of permafrost degradation (Verdonen et al., 2023), highlighting the importance

480 of abrupt thaw. While our study focuses on short-term CO_2 responses (three-month ~~incubation. However, a longer incubation period would be necessary to determine the time required for anaerobic conditions to establish in mesocosms, in contrast to traditional incubation vials (?). The increase~~ incubation) driven by hydrological differences between thaw types, these

processes also will likely differ in their temporal dynamics. Our results suggest that CO_2 emissions from abrupt thaw peak early and then stabilize and/or decrease as anaerobic conditions develop, whereas emissions from gradual thaw may increase more steadily as deeper layers thaw. The rise in CO_2 emissions from the Control during the final 10 days of incubation may ~~suggest the release of CO_2 from the permafrost layer~~ reflect this slower process (Table 2). Over longer timescales, palsas undergoing thaw (both abrupt and gradual) transition from initial CO_2 sources to net sinks as vegetation re-establishes and ecosystem productivity increases, a process that may take several decades (Johnston et al., 2014; Heffernan et al., 2022, 2024). This process is difficult to capture accurately under field conditions, highlighting the importance of continuous, long-term monitoring to assess CO_2 emissions during organic matter degradation — particularly before vegetation shifts and the onset of CH_4 emissions.

4.3 Comparison of Deeper Soil Contributions: Permafrost Degradation Simulation vs. Stabilized Thawed fen

C mineralization following permafrost thaw from peat partly depends on the stage of peat decomposition (Estop-Aragonés et al., 2022). Our FTIR results, along with soil parameters measured prior to incubation, indicate a higher potential for OM decomposition in the permafrost layer (>60 cm) compared to the active layer (~~0–60~~ 0-60 cm), as evidenced by higher pH values and reductions in CH and C=O peaks (Fig. 3, Fig. 4a). According to the post-incubation FTIR spectra and DI ratios, the highest decomposition occurred at the permafrost table (60 cm) under both flooded and dry conditions (Fig. 4b).This enhanced decomposition at the permafrost table can be attributed to the presence of active microbial communities—likely translocated from the active layer during thaw—and the availability of relatively undecomposed peat. In contrast, little to no peat decomposition occurred deeper within the permafrost layer (60–100 cm; Fig. 4b), despite the observed increase in CO_2 emissions under control conditions (Table 2). Furthermore, we observed minimal differences in the stage of peat decomposition between the deeper permafrost layer and the equivalent layer in the fen (60–100 cm; Fig. 3, Fig. 4a). This suggests that both the short-term thaw simulated in this study and 25 years of permafrost-free conditions have not significantly altered OM quality in the deeper permafrost layers (>60 cm). These findings are consistent with observations from other permafrost regions, such as in Canada (Harris et al., 2023). Thus, we conclude that peat degradation during permafrost thaw is primarily concentrated at the permafrost table, whereas in deeper layers, neither thaw processes nor long-term permafrost loss have notably affected peat quality.

Reif (2023) estimated that the fen site in Peera lost approximately 15 kg C $\cdot m^{-2}$ since thaw, without indicating any significant increase in peat decomposition at the fen site (Fig. 4a; Reif (2023)). This finding is consistent with Harris et al. (2023), who measured a net C loss of about 19.3 kg C $\cdot m^{-2}$ since thaw, with no observable changes in peat quality. Several studies have reported lower CO_2 emissions from degrading permafrost under waterlogged conditions (Estop-Aragonés et al., 2018a, b; Voigt et al., 2019), which could explain the minimal change in peat quality observed in the fen. This is in line with our observation of decreased CO_2 emissions per volume of thawed soil in the abrupt thaw simulation (flooded) and higher emissions in the gradual thaw simulation (Control) during the final thaw step (0–100 cm; Table 2). The greater contribution from deeper layers under control conditions may result from increased gas diffusivity in the drier soil column. However, without ^{14}C analysis, it

remains unclear whether emissions originate solely from the 80–100 cm layer or if the 60–80 cm layer contributed later due to lower diffusivity. Under flooded conditions, water saturation limits oxygen availability and slows gas diffusion (Voigt et al., 2019), leading to anaerobic conditions within the permafrost layer. Although microbial decomposition still occurs, it shifts to less efficient anaerobic pathways that produce CO_2 (along with other gases), which then accumulates due to restricted diffusion through the saturated soil.

In the fen mesocosms, CO_2 emissions increased with depth despite flooded conditions (Table 1, Fig. 6), with the highest DIs observed at the bottom of the cores (Fig. 4b). While surface vegetation was removed during incubation, the root systems were retained. The presence of deep-rooted aerenchymous plants, such as sedges, may explain the increased CO_2 emissions in the fen. Aerenchyma tissue enhances the transport of O_2, CO_2, and CH_4 in waterlogged soils (Armstrong, 1980; Colmer, 2003). Although aerenchyma are best known for enhancing CH_4 transport and reducing CH_4 oxidation, they can also provide pathways for CO_2 movement. Because CO_2 diffuses roughly 10,000 times faster in air than in water (Armstrong, 1980; Colmer, 2003; Tiner, 2005), gas exchange through aerenchyma can substantially influence CO_2 fluxes. In this process, O_2 is transported downward to the roots, while CO_2 produced by microbial activity moves upward and is fixed in the shoots via photosynthesis (Dacey and Klug, 1982; Pedersen and Sand-Jensen, 1992; Smith and Russell, 1969; Smith et al., 1983). In the absence of photosynthesis, roots may have acted as pathways for CO_2 from deeper layers. However, the artificial sequential thawing process may have amplified these emissions, leading to potential overestimation of CO_2 fluxes.

Finally, the degradation of dead roots could provide additional substrate, contributing to the higher DI observed at the bottom layer (Fig. 4b). This process may also increase soil porosity, facilitating gas exchange to the surface. This highlights the potential role of vegetation change since thaw in CO_2 transport, particularly when there is no active vegetation. While several studies have measured and modeled increased CO_2 emissions in northern fens during the non-growing and shoulder seasons (Fahnestock et al., 1999; Joiner et al., 1999; Natali et al., 2019; Rafat et al., 2021), few have accounted for the influence of vegetation type and root structure on CO_2 dynamics. This represents a significant gap in existing research and models, underscoring the need for further investigation in this area.

5 Conclusion

In conclusion, our findings contradicted our initial hypothesis by showing that the abrupt thaw simulation (i.e., flooding treatments) significantly enhanced CO_2 emissions with permafrost thaw, even when microbial communities had not yet adapted to saturated conditions (H1). This suggests that vertical ~~Ctransport~~ C transport, residual O_2, and redox changes induced by flooding play a crucial role in CO_2 dynamics during the thaw transition in abrupt palsa permafrost. By contrast, the composition of thermokarst thaw water appears to contribute less to C mineralization than the sudden increase in soil moisture (H2). Consistent with other studies, we observed an increase in CO_2 emissions only under gradual thaw simulations in thawing permafrost horizons. Additionally, ~~we detected a significant rise in~~ CO_2 emissions ~~in fens~~ from fens increased under water-saturated conditions ~~, likely driven by the often-overlooked role of deep-rooted vegetation in transporting~~ (H3), possibly reflecting CO_2 transport from deeper soil layers mediated by deep-rooted vegetation during non-growing and shoulder seasons. Our pilot

study underscores that substantial CO_2 emissions can be released during permafrost thaw, even under water-saturated conditions. Future research should focus on quantifying CO_2 release during abrupt thaw under in situ conditions. Additionally, model-based future projections should account for the potential contribution of greenhouse gases from deeper layers and the role of deep-rooted vegetation in producing and transporting CO_2 outside the growing season.

Data availability. The data sets used in this paper are available at doi: 10.1594/PANGAEA.974304 and doi: 10.1594/PANGAEA.974302

Author contributions. M.L., C.T. and J.Sch. designed the study. M.L., J.St. and T.W. collected the samples during the expedition in 2023. M.L. built the incubator and conducted the experiment, supported by M.Lü. M.H. and R.E. provided the laboratory infrastructure and the original script for the flux calculations. M.L. carried out the data analyses and M.H. provided the script. M.B. assisted with data interpretation. M.L. wrote the manuscript with contributions from all the co-authors.

Competing interests. The authors declare no conflict of interest.

Acknowledgements. This study was funded by the Alfred Wegener Institute (grant details: INSPIRES PhD Fellowship) and the European Research Council (ERC grant: FluxWIN Project 851181). We are grateful to the Research Station of Kilpisjärvi for their assistance during fieldwork. We would like to acknowledge J. Vollmer, M. Dolle and S. Wocheslander, as well as the AWI lab technicians, for their support with laboratory work. We also thank our colleagues for their valuable discussions and feedback. Finally, we extend our gratitude to the reviewers whose comments helped improve this manuscript.

565 References

Armstrong, W.: Aeration in higher plants, in: Advances in botanical research, vol. 7, pp. 225–332, Elsevier, 1980.

Baysinger, M., Laurent, M., Verdonen, M., Reif, J., Kumpula, T., Liebner, S., and Treat, C.: Abrupt thaw in a Finnish palsa: Potential CH4 production driven by vegetation adaptation in the transition from permafrost to post-thaw soils, Journal of Geophysical Research: Biogeosciences, 130, e2025JG008 847, 2025.

570 Borge, A. F., Westermann, S., Solheim, I., and Etzelmüller, B.: Strong degradation of palsas and peat plateaus in northern Norway during the last 60 years, The Cryosphere, 11, 1–16, 2017.

Camill, P.: Peat accumulation and succession following permafrost thaw in the boreal peatlands of Manitoba, Canada, Ecoscience, 6, 592–602, 1999.

Capriel, P., Beck, T., Borchert, H., Gronholz, J., and Zachmann, G.: Hydrophobicity of the organic matter in arable soils, Soil Biology and
575 Biochemistry, 27, 1453–1458, 1995.

Chanton, J., Glaser, P., Chasar, L., Burdige, D. J., Hines, M., Siegel, D., Tremblay, L., and Cooper, W.: Radiocarbon evidence for the importance of surface vegetation on fermentation and methanogenesis in contrasting types of boreal peatlands, Global Biogeochemical Cycles, 22, 2008.

Chen, C., Hall, S. J., Coward, E., and Thompson, A.: Iron-mediated organic matter decomposition in humid soils can counteract protection,
580 Nature communications, 11, 2255, 2020.

Clein, J. S. and Schimel, J. P.: Reduction in microbial activity in Birch litter due to drying and rewetting event, Soil Biology and Biochemistry, 26, 403–406, 1994.

Colmer, T.: Long-distance transport of gases in plants: a perspective on internal aeration and radial oxygen loss from roots, Plant, Cell & Environment, 26, 17–36, 2003.

585 Cooper, M. D., Estop-Aragonés, C., Fisher, J. P., Thierry, A., Garnett, M. H., Charman, D. J., Murton, J. B., Phoenix, G. K., Treharne, R., Kokelj, S. V., et al.: Limited contribution of permafrost carbon to methane release from thawing peatlands, Nature Climate Change, 7, 507–511, 2017.

Crevecoeur, S., Vincent, W. F., Comte, J., and Lovejoy, C.: Bacterial community structure across environmental gradients in permafrost thaw ponds: methanotroph-rich ecosystems, Frontiers in microbiology, 6, 192, 2015.

590 Dacey, J. and Klug, M.: Tracer transport in Nuphar: $^{18}O_2$ and $^{14}CO_2$ transport, Physiologia Plantarum, 56, 361–366, 1982.

Denef, K., Six, J., Paustian, K., and Merckx, R.: Importance of macroaggregate dynamics in controlling soil carbon stabilization: short-term effects of physical disturbance induced by dry–wet cycles, Soil Biology and Biochemistry, 33, 2145–2153, 2001.

Ellerbrock, R. and Kaiser, M.: Stability and composition of different soluble soil organic matter fractions–evidence from δ13C and FTIR signatures, Geoderma, 128, 28–37, 2005.

595 Ellerbrock, R. H. and Gerke, H. H.: Characterization of organic matter composition of soil and flow path surfaces based on physicochemical principles—A review, Advances in agronomy, 121, 117–177, 2013.

Ellerbrock, R. H. and Gerke, H. H.: FTIR spectral band shifts explained by OM–cation interactions, Journal of Plant Nutrition and Soil Science, 184, 388–397, 2021.

Ellerbrock, R. H., Höhn, A., and Gerke, H.: Characterization of soil organic matter from a sandy soil in relation to management practice
600 using FT-IR spectroscopy, Plant and Soil, 213, 55–61, 1999.

Ellerbrock, R. H., Gerke, H. H., and Böhm, C.: In situ DRIFT characterization of organic matter composition on soil structural surfaces, Soil Science Society of America Journal, 73, 531–540, 2009.

Ellerbrock, R. H., Niessner, D., Deumlich, D., Puppe, D., and Gerke, H. H.: Infrared-based analysis of organic matter composition in liquid and solid runoff fractions collected during a single erosion event, Soil and Tillage Research, 235, 105 901, 2024.

605   Estop-Aragonés, C., Cooper, M. D., Fisher, J. P., Thierry, A., Garnett, M. H., Charman, D. J., Murton, J. B., Phoenix, G. K., Treharne, R., Sanderson, N. K., et al.: Limited release of previously-frozen C and increased new peat formation after thaw in permafrost peatlands, Soil Biology and Biochemistry, 118, 115–129, 2018a.

Estop-Aragonés, C., Czimczik, C. I., Heffernan, L., Gibson, C., Walker, J. C., Xu, X., and Olefeldt, D.: Respiration of aged soil carbon during fall in permafrost peatlands enhanced by active layer deepening following wildfire but limited following thermokarst, Environmental

610   Research Letters, 13, 085 002, 2018b.

Estop-Aragonés, C., Heffernan, L., Knorr, K.-H., and Olefeldt, D.: Limited potential for mineralization of permafrost peatland soil carbon following thermokarst: evidence from anoxic incubation and priming experiments, Journal of Geophysical Research: Biogeosciences, 127, e2022JG006 910, 2022.

Fahnestock, J. T., Jones, M. H., and Welker, J. M.: Wintertime CO2 efflux from arctic soils: implications for annual carbon budgets, Global

615   Biogeochemical Cycles, 13, 775–779, 1999.

Fewster, R. E., Morris, P. J., Ivanovic, R. F., Swindles, G. T., Peregon, A. M., and Smith, C. J.: Imminent loss of climate space for permafrost peatlands in Europe and Western Siberia, Nature Climate Change, 12, 373–379, 2022.

Fierer, N. and Schimel, J. P.: A proposed mechanism for the pulse in carbon dioxide production commonly observed following the rapid rewetting of a dry soil, Soil Science Society of America Journal, 67, 798–805, 2003.

620   Frolking, S. and Roulet, N. T.: Holocene radiative forcing impact of northern peatland carbon accumulation and methane emissions, Global Change Biology, 13, 1079–1088, 2007.

Haberhauer, G. and Gerzabek, M.: Drift and transmission FT-IR spectroscopy of forest soils: an approach to determine decomposition processes of forest litter, Vibrational Spectroscopy, 19, 413–417, 1999.

Han, L., Sun, K., Jin, J., and Xing, B.: Some concepts of soil organic carbon characteristics and mineral interaction from a review of literature,

625   Soil Biology and Biochemistry, 94, 107–121, 2016.

Harris, L. I., Olefeldt, D., Pelletier, N., Blodau, C., Knorr, K.-H., Talbot, J., Heffernan, L., and Turetsky, M.: Permafrost thaw causes large carbon loss in boreal peatlands while changes to peat quality are limited, Global Change Biology, 29, 5720–5735, 2023.

Heffernan, L., Estop-Aragonés, C., Knorr, K.-H., Talbot, J., and Olefeldt, D.: Long-term impacts of permafrost thaw on carbon storage in peatlands: Deep losses offset by surficial accumulation, Journal of Geophysical Research: Biogeosciences, 125, e2019JG005 501, 2020.

630   Heffernan, L., Cavaco, M. A., Bhatia, M. P., Estop-Aragonés, C., Knorr, K.-H., and Olefeldt, D.: High peatland methane emissions following permafrost thaw: enhanced acetoclastic methanogenesis during early successional stages, Biogeosciences Discussions, 2022, 1–49, 2022.

Heffernan, L., Estop-Aragonés, C., Kuhn, M. A., Holger-Knorr, K., and Olefeldt, D.: Changing climatic controls on the greenhouse gas balance of thermokarst bogs during succession after permafrost thaw, Global Change Biology, 30, e17 388, 2024.

Heller, C., Ellerbrock, R., Roßkopf, N., Klingenfuß, C., and Zeitz, J.: Soil organic matter characterization of temperate peatland soil with

635   FTIR-spectroscopy: effects of mire type and drainage intensity, European Journal of Soil Science, 66, 847–858, 2015.

Hodgkins, S. B., Tfaily, M. M., McCalley, C. K., Logan, T. A., Crill, P. M., Saleska, S. R., Rich, V. I., and Chanton, J. P.: Changes in peat chemistry associated with permafrost thaw increase greenhouse gas production, Proceedings of the National Academy of Sciences, 111, 5819–5824, 2014.

Hoffmann, M., Jurisch, N., Garcia Alba, J., Albiac Borraz, E., Schmidt, M., Huth, V., Rogasik, H., Rieckh, H., Verch, G., Sommer, M., et al.: Detecting small-scale spatial heterogeneity and temporal dynamics of soil organic carbon (SOC) stocks: a comparison between automatic chamber-derived C budgets and repeated soil inventories, Biogeosciences, 14, 1003–1019, 2017.

Holmes, M., Crill, P., Burnett, W., McCalley, C., Wilson, R., Frolking, S., Chang, K.-Y., Riley, W., Varner, R., Hodgkins, S., et al.: Carbon accumulation, flux, and fate in Stordalen Mire, a permafrost peatland in transition, Global Biogeochemical Cycles, 36, e2021GB007 113, 2022.

Hugelius, G., Loisel, J., Chadburn, S., Jackson, R. B., Jones, M., MacDonald, G., Marushchak, M., Olefeldt, D., Packalen, M., Siewert, M. B., et al.: Large stocks of peatland carbon and nitrogen are vulnerable to permafrost thaw, Proceedings of the National Academy of Sciences, 117, 20 438–20 446, 2020.

Johnston, C. E., Ewing, S. A., Harden, J. W., Varner, R. K., Wickland, K. P., Koch, J. C., Fuller, C. C., Manies, K., and Jorgenson, M. T.: Effect of permafrost thaw on CO_2 and CH_4 exchange in a western Alaska peatland chronosequence, Environmental Research Letters, 9, 085 004, 2014.

Joiner, D. W., Lafleur, P. M., McCaughey, J. H., and Bartlett, P. A.: Interannual variability in carbon dioxide exchanges at a boreal wetland in the BOREAS northern study area, Journal of Geophysical Research: Atmospheres, 104, 27 663–27 672, 1999.

Jones, M. C., Harden, J., O'Donnell, J., Manies, K., Jorgenson, T., Treat, C., and Ewing, S.: Rapid carbon loss and slow recovery following permafrost thaw in boreal peatlands, Global change biology, 23, 1109–1127, 2017.

Jorgenson, M. T., Shur, Y. L., and Pullman, E. R.: Abrupt increase in permafrost degradation in Arctic Alaska, Geophysical Research Letters, 33, L02 503, https://doi.org/10.1029/2005GL024960, 2006.

Kim, D.-G., Mu, S., Kang, S., and Lee, D.: Factors controlling soil CO_2 effluxes and the effects of rewetting on effluxes in adjacent deciduous, coniferous, and mixed forests in Korea, Soil Biology and Biochemistry, 42, 576–585, 2010.

Kim, D.-G., Vargas, R., Bond-Lamberty, B., and Turetsky, M.: Effects of soil rewetting and thawing on soil gas fluxes: a review of current literature and suggestions for future research, Biogeosciences, 9, 2459–2483, 2012.

Kirkwood, A., Roy-Léveillée, P., Packalen, M. S., McLaughlin, J., and Basiliko, N.: Evolution of Palsas and Peat Plateaus in the Hudson Bay Lowlands: Permafrost Degradation and the Production of Greenhouse Gases, Cold Regions Engineering 2019, https://api.semanticscholar.org/CorpusID:214103536, 2019.

Kirkwood, J. A. H., Roy-Léveillée, P., Mykytczuk, N., Packalen, M., McLaughlin, J., Laframboise, A., and Basiliko, N.: Soil microbial community response to permafrost degradation in palsa fields of the Hudson Bay Lowlands: Implications for greenhouse gas production in a warming climate, Global Biogeochemical Cycles, 35, e2021GB006 954, 2021.

Kjær, S. T., Westermann, S., Nedkvitne, N., and Dörsch, P.: Carbon degradation and mobilisation potentials of thawing permafrost peatlands in northern Norway inferred from laboratory incubations, Biogeosciences, 21, 4723–4737, 2024.

Könönen, O. H., Karjalainen, O., Aalto, J., Luoto, M., and Hjort, J.: Environmental spaces for palsas and peat plateaus are disappearing at a circumpolar scale, The Cryosphere Discussions, 2022, 1–37, 2022.

Kuhn, M., Lundin, E. J., Giesler, R., Johansson, M., and Karlsson, J.: Emissions from thaw ponds largely offset the carbon sink of northern permafrost wetlands, Scientific Reports, 8, 9535, 2018.

Kurylyk, B. L., Hayashi, M., Quinton, W. L., McKenzie, J. M., and Voss, C. I.: Influence of vertical and lateral heat transfer on permafrost thaw, peatland landscape transition, and groundwater flow, Water Resources Research, 52, 1286–1305, 2016.

Laurent, M., Lück, M., and Treat, C. C.: Continuous CO_2, CH_4 and H_2O fluxes measured during a 3-month mesocosm incubation from a Palsa, https://doi.pangaea.de/10.1594/PANGAEA.974302, dataset in review, 2025a.

Laurent, M., Lück, M., and Treat, C. C.: Initial soil parameters of a palsa and a peatland core used in a mesocosm incubation, https://doi.pangaea.de/10.1594/PANGAEA.974304, dataset in review, 2025b.

Lee, C.: Controls on organic carbon preservation: The use of stratified water bodies to compare intrinsic rates of decomposition in oxic and anoxic systems, Geochimica et Cosmochimica Acta, 56, 3323–3335, 1992.

Leppiniemi, O., Karjalainen, O., Aalto, J., Yletyinen, E., Luoto, M., and Hjort, J.: The morpho-ecological state of palsa mires in sub-arctic Fennoscandia: insights from high-resolution spatial modelling, Catena, 257, 109 203, 2025.

Leroy, M., Burnett, M. S., Laurion, I., Douglas, P. M., Kallenbach, C. M., and Comte, J.: Terrestrial-aquatic connectivity structures microbial communities during the formation of thermokarst lakes, ISME Communications, p. ycaf027, 2025.

Malhotra, A. and Roulet, N.: Environmental correlates of peatland carbon fluxes in a thawing landscape: do transitional thaw stages matter?, Biogeosciences, 12, 3119–3130, 2015.

Mastepanov, M. and Christensen, T. R.: Laboratory investigations of methane buildup in, and release from, shallow peats, Carbon Cycling in Northern Peatlands, 184, 205–218, 2009.

Matveev, A., Laurion, I., Deshpande, B. N., Bhiry, N., and Vincent, W. F.: High methane emissions from thermokarst lakes in subarctic peatlands, Limnology and Oceanography, 61, S150–S164, 2016.

McGuire, A. D., Anderson, L. G., Christensen, T. R., Dallimore, S., Guo, L., Hayes, D. J., Heimann, M., Lorenson, T. D., Macdonald, R. W., and Roulet, N.: Sensitivity of the carbon cycle in the Arctic to climate change, Ecological monographs, 79, 523–555, 2009.

Mellegård, H., Stalheim, T., Hormazabal, V., Granum, P., and Hardy, S.: Antibacterial activity of sphagnum acid and other phenolic compounds found in Sphagnum papillosum against food-borne bacteria, Letters in applied microbiology, 49, 85–90, 2009.

Natali, S. M., Watts, J. D., Rogers, B. M., Potter, S., Ludwig, S. M., Selbmann, A.-K., Sullivan, P. F., Abbott, B. W., Arndt, K. A., Birch, L., et al.: Large loss of CO2 in winter observed across the northern permafrost region, Nature Climate Change, 9, 852–857, 2019.

Nickerson, N.: Evaluating gas emission measurements using Minimum Detectable Flux (MDF), Eosense Inc., Dartmouth, Nova Scotia, Canada, 2016.

Obu, J., Westermann, S., Bartsch, A., Berdnikov, N., Christiansen, H. H., Dashtseren, A., Delaloye, R., Elberling, B., Etzelmüller, B., Kholodov, A., et al.: Northern Hemisphere permafrost map based on TTOP modelling for 2000–2016 at 1 km2 scale, Earth-Science Reviews, 193, 299–316, 2019.

Olefeldt, D., Heffernan, L., Jones, M. C., Sannel, A. B. K., Treat, C. C., and Turetsky, M. R.: Permafrost thaw in northern peatlands: rapid changes in ecosystem and landscape functions, Ecosystem collapse and climate change, pp. 27–67, 2021.

Olvmo, M., Holmer, B., Thorsson, S., Reese, H., and Lindberg, F.: Sub-arctic palsa degradation and the role of climatic drivers in the largest coherent palsa mire complex in Sweden (Vissátvuopmi), 1955–2016, Scientific reports, 10, 8937, 2020.

Patzner, M. S., Mueller, C. W., Malusova, M., Baur, M., Nikeleit, V., Scholten, T., Hoeschen, C., Byrne, J. M., Borch, T., Kappler, A., and Bryce, C.: Iron mineral dissolution releases iron and associated organic carbon during permafrost thaw, Nature Communications, 11, 6329, https://doi.org/10.1038/s41467-020-20102-6, 2020.

Pedersen, O. and Sand-Jensen, K.: Adaptations of submerged Lobelia dortmanna to aerial life form: morphology, carbon sources and oxygen dynamics, Oikos, pp. 89–96, 1992.

Peura, S., Wauthy, M., Simone, D., Eiler, A., Einarsdóttir, K., Rautio, M., and Bertilsson, S.: Ontogenic succession of thermokarst thaw ponds is linked to dissolved organic matter quality and microbial degradation potential, Limnology and Oceanography, 65, S248–S263, 2020.

Quinton, W. L. and Baltzer, J.: The active-layer hydrology of a peat plateau with thawing permafrost (Scotty Creek, Canada), Hydrogeology Journal, 21, 201, 2013.

R Core Team: R: A Language and Environment for Statistical Computing, R Foundation for Statistical Computing, Vienna, Austria, https://www.R-project.org/, 2024.

Rafat, A., Rezanezhad, F., Quinton, W. L., Humphreys, E. R., Webster, K., and Van Cappellen, P.: Non-growing season carbon emissions in a northern peatland are projected to increase under global warming, Communications Earth & Environment, 2, 111, 2021.

Rantanen, M., Karpechko, A. Y., Lipponen, A., Nordling, K., Hyvärinen, O., Ruosteenoja, K., Vihma, T., and Laaksonen, A.: The Arctic has warmed nearly four times faster than the globe since 1979, Communications earth & environment, 3, 168, 2022.

Reddy, K. R. and DeLaune, R. D.: Biogeochemistry of wetlands: science and applications, CRC Press, Boca Raton, ISBN 978-1-56670-678-0, 2008.

Reif, J.: Carbon dynamics following permafrost thaw gradient in a high latitude peatland environment, 2023.

Rodenhizer, H., Natali, S. M., Mauritz, M., Taylor, M. A., Celis, G., Kadej, S., Kelley, A. K., Lathrop, E. R., Ledman, J., Pegoraro, E. F., Salmon, V. G., Schädel, C., See, C., Webb, E. E., and Schuur, E. A. G.: Abrupt permafrost thaw drives spatially heterogeneous soil moisture and carbon dioxide fluxes in upland tundra, Global Change Biology, p. gcb.16936, https://doi.org/10.1111/gcb.16936, 2023a.

Rodenhizer, H., Natali, S. M., Mauritz, M., Taylor, M. A., Celis, G., Kadej, S., Kelley, A. K., Lathrop, E. R., Ledman, J., Pegoraro, E. F., et al.: Abrupt permafrost thaw drives spatially heterogeneous soil moisture and carbon dioxide fluxes in upland tundra, Global change biology, 29, 6286–6302, 2023b.

Rodionov, S. N.: A sequential algorithm for testing climate regime shifts, Geophysical Research Letters, 31, 2004.

Room, A. H., Franco-Gaviria, F., and Urrego, D. H.: rshift: paleoecology and regime shift analysis, https://CRAN.R-project.org/package=rshift, 2020.

Sannel, A. B. K. and Kuhry, P.: Holocene peat growth and decay dynamics in sub-arctic peat plateaus, west-central Canada, Boreas, 38, 13–24, 2009.

Schuur, E. A. G., Bockheim, J., Canadell, J. G., Euskirchen, E., Field, C. B., Goryachkin, S. V., Hagemann, S., Kuhry, P., Lafleur, P. M., Lee, H., Mazhitova, G., Nelson, F. E., Rinke, A., Romanovsky, V. E., Shiklomanov, N., Tarnocai, C., Venevsky, S., Vogel, J. G., and Zimov, S. A.: Vulnerability of Permafrost Carbon to Climate Change: Implications for the Global Carbon Cycle, BioScience, 58, 701–714, https://doi.org/10.1641/B580807, 2008.

Seppälä, M.: The origin of palsas, Geografiska Annaler: Series A, Physical Geography, 68, 141–147, 1986.

Smith, C., DeLaune, R., and Patrick, W.: Carbon dioxide emission and carbon accumulation in coastal wetlands, Estuarine, Coastal and Shelf Science, 17, 21–29, https://doi.org/10.1016/0272-7714(83)90042-2, 1983.

Smith, K. and Russell, R. S.: Occurrence of ethylene, and its significance, in anaerobic soil, Nature, 222, 769–771, 1969.

Smith, S. L., O'Neill, H. B., Isaksen, K., Noetzli, J., and Romanovsky, V. E.: The changing thermal state of permafrost, Nature Reviews Earth & Environment, 3, 10–23, 2022.

Tfaily, M. M., Wilson, R. M., Cooper, W. T., Kostka, J. E., Hanson, P., and Chanton, J. P.: Vertical stratification of peat pore water dissolved organic matter composition in a peat bog in northern Minnesota, Journal of Geophysical Research: Biogeosciences, 123, 479–494, 2018.

Tiner, R. W.: In search of swampland: a wetland sourcebook and field guide, Rutgers University Press, ISBN 978-0-8135-3681-1, 2005.

Treat, C. C., Wollheim, W. M., Varner, R. K., Grandy, A. S., Talbot, J., and Frolking, S.: Temperature and peat type control CO_2 and CH_4 production in Alaskan permafrost peats, Global Change Biology, 20, 2674–2686, https://doi.org/10.1111/gcb.12572, 2014.

Treat, C. C., Ernakovich, J., Iversen, C. M., Lupascu, M., McGuire, A. D., Norby, R. J., Roy Chowdhury, T., Richter, A., Šantrůčková, H., Schädel, C., Schuur, E. A. G., Sloan, V. L., Turetsky, M. R., and Waldrop, M. P.: A pan-Arctic synthesis of CH_4 and CO_2 production from anoxic soil incubations, Global Change Biology, 21, 2787–2803, https://doi.org/10.1111/gcb.12875, 2015.

Treat, C. C., Jones, M. C., Alder, J., Sannel, A. B. K., Camill, P., and Frolking, S.: Predicted vulnerability of carbon in permafrost peatlands with future climate change and permafrost thaw in Western Canada, Journal of Geophysical Research: Biogeosciences, 126, e2020JG005 872, 2021.

Turetsky, M., Wieder, R., Vitt, D., Evans, R., and Scott, K.: The disappearance of relict permafrost in boreal north America: Effects on peatland carbon storage and fluxes, Global Change Biology, 13, 1922–1934, 2007.

Turetsky, M. R., Wieder, R. K., Williams, C. J., and Vitt, D. H.: Organic matter accumulation, peat chemistry, and permafrost melting in peatlands of boreal Alberta, Ecoscience, 7, 115–122, 2000.

Turetsky, M. R., Wieder, R. K., and Vitt, D. H.: Boreal peatland C fluxes under varying permafrost regimes, Soil Biology and Biochemistry, 34, 907–912, 2002.

Turetsky, M. R., Abbott, B. W., Jones, M. C., Anthony, K. W., Olefeldt, D., Schuur, E. A., Grosse, G., Kuhry, P., Hugelius, G., Koven, C., et al.: Carbon release through abrupt permafrost thaw, Nature Geoscience, 13, 138–143, 2020.

Van Gestel, M., Merckx, R., and Vlassak, K.: Microbial biomass responses to soil drying and rewetting: the fate of fast-and slow-growing microorganisms in soils from different climates, Soil Biology and Biochemistry, 25, 109–123, 1993.

Verdonen, M., Störmer, A., Lotsari, E., Korpelainen, P., Burkhard, B., Colpaert, A., and Kumpula, T.: Permafrost degradation at two monitored palsa mires in north-west Finland, The Cryosphere, 17, 1803–1819, 2023.

Voigt, C., Lamprecht, R. E., Marushchak, M. E., Lind, S. E., Novakovskiy, A., Aurela, M., Martikainen, P. J., and Biasi, C.: Warming of subarctic tundra increases emissions of all three important greenhouse gases–carbon dioxide, methane, and nitrous oxide, Global Change Biology, 23, 3121–3138, 2017.

Voigt, C., Marushchak, M. E., Mastepanov, M., Lamprecht, R. E., Christensen, T. R., Dorodnikov, M., Jackowicz-Korczyński, M., Lindgren, A., Lohila, A., Nykänen, H., Oinonen, M., Oksanen, T., Palonen, V., Treat, C. C., Martikainen, P. J., and Biasi, C.: Ecosystem carbon response of an Arctic peatland to simulated permafrost thaw, Global Change Biology, 25, 1746–1764, https://doi.org/10.1111/gcb.14574, 2019.

Webb, H., Fuchs, M., Abbott, B. W., Douglas, T., Elder, C., Ernakovich, J. G., Euskirchen, E. S., Göckede, M., Grosse, G., Hugelius, G., Jones, M. C., Koven, C., Kropp, H., Lathrop, E., Li, W., Loranty, M. M., Natali, S. M., Olefeldt, D., Schädel, C., Schuur, E., Sonnentag, O., Strauss, J., Virkkala, A.-M., and Turetsky, M.: A review of abrupt permafrost thaw: Definitions, usage, and a proposed conceptual framework, Current Climate Change Reports, accepted, 2025.

Xiang, S.-R., Doyle, A., Holden, P. A., and Schimel, J. P.: Drying and rewetting effects on C and N mineralization and microbial activity in surface and subsurface California grassland soils, Soil biology and biochemistry, 40, 2281–2289, 2008.

Zaitseva, N. et al.: A polysaccharide extracted from Sphagnum moss as antifungal agent in archaeological conservation, in: Masters Abstracts International, vol. 49, 2010.